# Chapter 10
# Examples of Applications

The examples of the calculations of the selected engineering problems given in this Chapter demonstrate the practice of numerical solutions. In real structures we always ask questions as to what geometry and what values of the material data are appropriate to pass from the physical model of the structure to the numerical one. Real shapes are usually complex and we try to simplify them, replacing curves with straight lines, non-uniformly distributed material parameters with homogeneous material, material damping with a numerical decay of the amplitude. Let us consider, as a first example, a track subjected to a moving vehicle. We can build a detailed three-dimensional model using cubes or tetrahedra with many degrees of freedom describing the foundation, ballast, track elements, rails, wheels, and the remaining part of the vehicle. We can include contact phenomena, friction, material nonlinearities, thermo-mechanical coupling, etc. However, such a model nowadays would be a challenge even for a static problem. Calculating the solution can last even a quarter of an hour. That is relatively long considering the computational power of multi-core processors. In a dynamic analysis, such a computation must be repeated thousands of times. The duration of the task exceeds any reasonable length of time. That is why we must still simplify our numerical models and improve the computational tools. Fortunately, a coarse discretization and a simplified mesh does not influence the frequencies significantly. The amplitudes are worse.

In vibration analysis of structures under moving loads we often search for the interaction of the moving vehicle and the load-carrying structure. In the case of multipoint contact of a base with a multi degree-of-freedom vehicle, such interactions are essential.

The problem of ill-conditioned systems of algebraic equations is well known in computer analysis. Especially, the assumption of constants whose ranges vary several times may cause problems. If the commercial software recalculates the given data to scaled values, we can partly trust the solutions. This issue is essential since in dynamic simulations the computational error can occur at least once during each step of the computations and, in an initially invisible way, affect severly the final results. In complex problems, we will not be able to detect such incorrect solutions. In the case of custom-written computer programs we ourselves should ensure that

C.I. Bajer and B. Dyniewicz: Numerical Analysis of Vibrations of Structures, LNACM 65, pp. 247–270.
springerlink.com
© Springer-Verlag Berlin Heidelberg 2012

**Table 10.1** Material data of structural elements.

| parameter | value [SI units] | value [cm, g, $\mu$s] |
|---|---|---|
| rail | | |
| $E$ | 210 GPa | 2.1 |
| $A$ | $7.7{\cdot}10^{-3}$ m$^2$ | 77. |
| $\nu$ | 0.2 | 0.2 |
| $\rho$ | 7860 kg/m$^3$ | 7.86 |
| $G$ | 77 GPa | 0.77 |
| $I$ | $30.55{\cdot}10^{-6}$ m$^4$ | 3055. |
| elastic pad | | |
| $E$ | 0.25–0.50 GPa | $2.5{\cdot}10^{-3}$–$5.0{\cdot}10^{-3}$ |
| $A$ | $22.5{\cdot}10^{-3}$ m$^2$ | 225. |
| $\rho$ | 1800 kg/m$^3$ | 1.8 |
| sleeper (concrete) | | |
| $E$ | 30 GPa | 0.3 |
| $G$ | 7.7 GPa | 0.077 |
| $A$ | $15{\cdot}10^{-3}$ m$^2$ | 150. |
| $\rho$ | 2400 kg/m$^3$ | 2.4 |
| sleeper (wooden) | | |
| $E$ | 11 GPa | 0.11 |
| $A$ | $35{\cdot}10^{-3}$ m$^2$ | 350. |
| $\rho$ | 0.65 g/cm$^3$ | 0.65 |
| Y-type sleeper (steel) | | |
| $E$ | 210 GPa | 2.1 |
| $A$ | $21.6{\cdot}10^{-3}$ m$^2$ | 216. |
| $\rho$ | 7860 kg/m$^3$ | 7.86 |
| ground | | |
| $k_z$ (soft) | $10^5$ Pa | $10^{-6}$ |
| $k_z$ (sand compacted) | $10^8$ Pa | $10^{-3}$ |
| $k_z$ (rigid) | $10^{10}$ Pa | $10^{-1}$ |
| $\nu$ | 0.3 | 0.3 |
| ballast | | |
| $E$ | 500 MPa | $5{\cdot}10^{-3}$ |
| $\rho$ | $>$1200 kg/m$^3$ | $>$1.2 |
| $\nu$ | 0.3 | 0.3 |

the matrices in our systems of equations are well-conditioned. The simplest way is to deliver the data, both geometric and material, within a similar range. For this purpose, it is better to replace the SI system of units by another one, more suitable. We chose the following system of units: cm, g, $\mu$s. This results in most of data's having almost the same range, especially the Young modulus and the time step.

**Table 10.2** Data assumed in simulation.

| | |
|---|---|
| rail UIC-60 bending stiffness EI | 6.42 MN/m$^2$ |
| mass density per unit length $\rho A$ | 60 kg/m |
| damping loss factor of rail $\eta_r$ | 0.02 |
| stiffness of elastic pad per unit length | 300 MN/m$^2$ |
| damping loss factor of a pad $\eta_p$ | 0.2 |
| sleeper mass per unit length of a track (per one rail) | 250 kg/m |
| ballast stiffness per unit length of a track (one rail) | 100 MN/m$^2$ |
| ballast damping loss factor $\eta_b$ | 1.0 |
| foundation damping loss factor $\eta_f$ | 0.1 |

Below we will give the material data useful for simulations of railway problems. All the values are given both in the SI system and in our system of units. In Table 10.1 one can find the data for the fundamental types of elements of the track. The material and structural data assumed in the further simulation is collected in Table 10.2.

## 10.1 Dynamics of the Classical Vehicle–Track System

Now let us have a look at the real example of vibrations of a carriage moving on a classical track. The custom computer software used here was written by the authors, implementing the numerical approaches given in this book. We use the geometric and material data from [42].

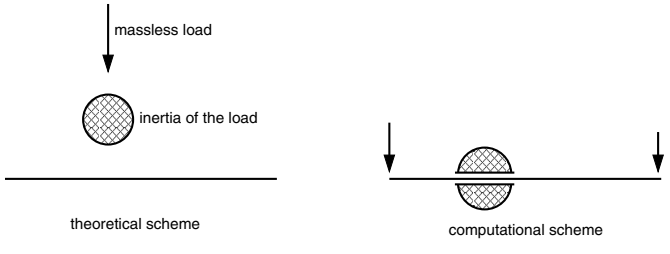


**Fig. 10.1** Theoretical scheme of the problem and the scheme assumed for computations.

The replacement of the real physical load with the computational load is explained in Figure 10.1. The finite element is subjected at the intermediate point to the force with the inertia parameter, i.e., the concentrated mass. This force, usually placed in a numerical model at the right-hand side of the resulting system of algebraic equations, can be simply distributed over the neighbouring nodes. The bending moments in the case of a beam must appear at the finite element joints as well. The concentrated mass is incorporated directly into the left-hand side matrices. Their coefficients vary in each time step and this requires the solution of a

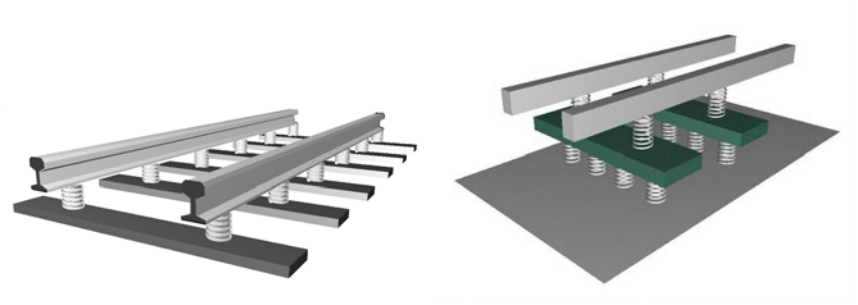

**Fig. 10.2** Substructures assumed in analysis.

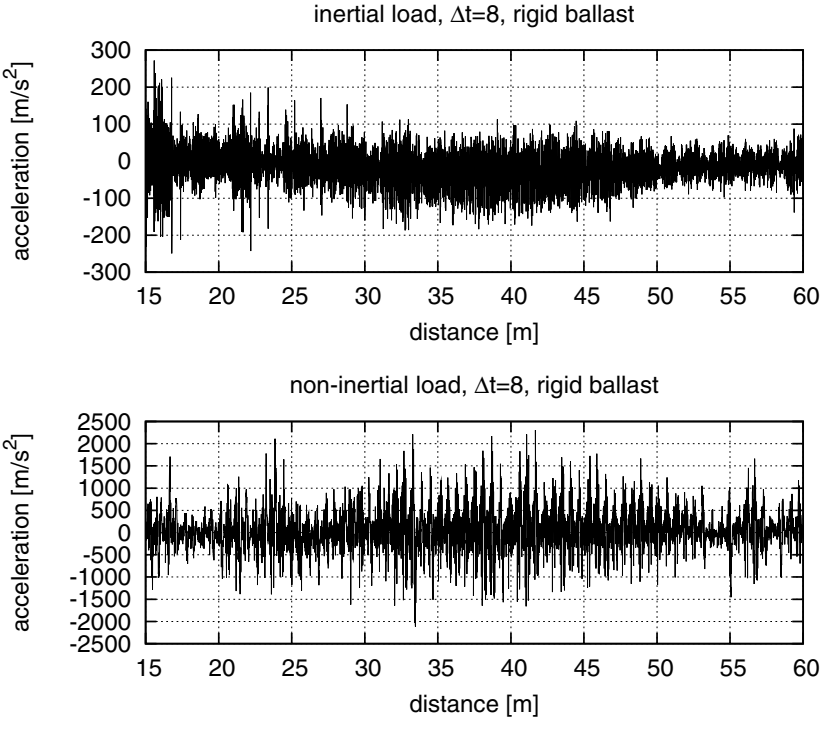


**Fig. 10.3** Vertical accelerations of the axle box at a speed of 290 km/h with the inertial and non-inertial loads assumed in the model.

system of equations at every time step. No iterations are required, unless unilateral contact is assumed. There are two advantages of such a solution: accurate and faster computations.

The track model is composed of plates, beams, grid or frame elements, and springs. A simple track structure can be considered in the same manner as a

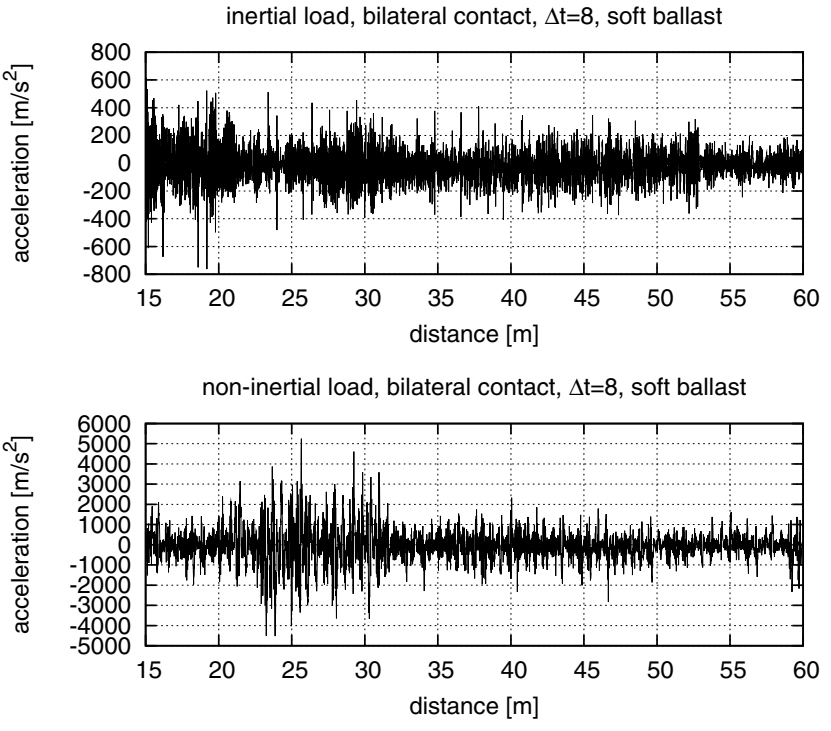


**Fig. 10.4** Vertical accelerations of the axle box at a speed of 290 km/h with the inertial and non-inertial loads assumed in the model with soft ballast.

complex one. Let us look at the simplest classical track (Figure 10.2), built of sleepers as grid elements placed on an elastic Winkler foundation, springs which model elastic pads, and grid elements which describe rails, both straight and curved. In both Figures 10.3 and 10.4 in the case of a non-inertial load (lower diagrams) we can notice the strong influence of the sleepers. With an inertial load (upper plots), this influence is moderate and the dynamic response is more realistic.

We can compare our results with the reference paper [42] (Figure 10.5). Both Figures 10.3 and 10.5, obtained for an inertial load, exhibit a similar range of accelerations of the axle box. The signal in Figure 10.5 shows a low frequency mode which is difficult to explain. The response of our numerical simulation has the same magnitude of accelerations and has more realistic higher frequency oscillations. The model analysis of the plotted signal is depicted in Figure 10.6. Figure 10.7 shows the accelerations of the car's body at a speed of 290 km/h.

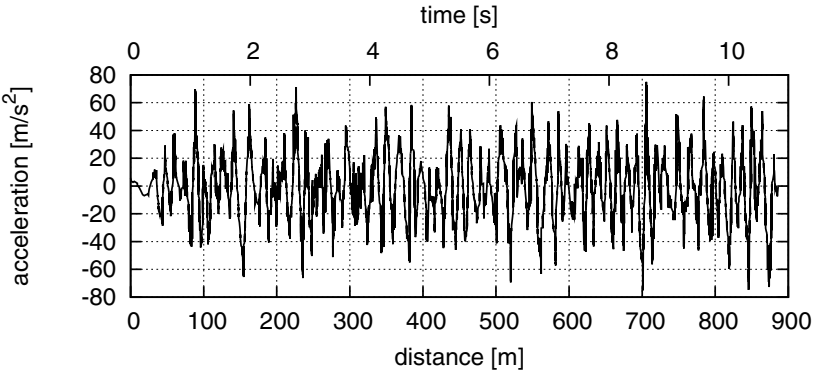


**Fig. 10.5** Accelerations of the axle box at a speed of 290 km/h taken from [42].

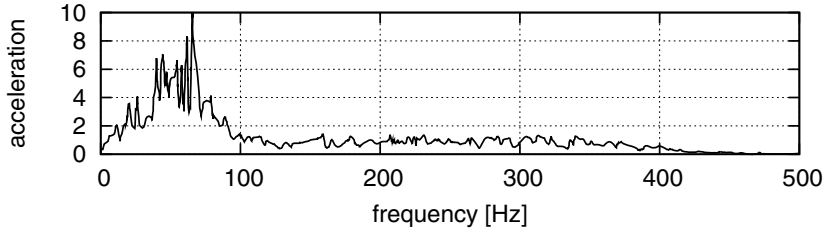


**Fig. 10.6** Modal analysis of the acceleration signal from Figure 10.5 [42].

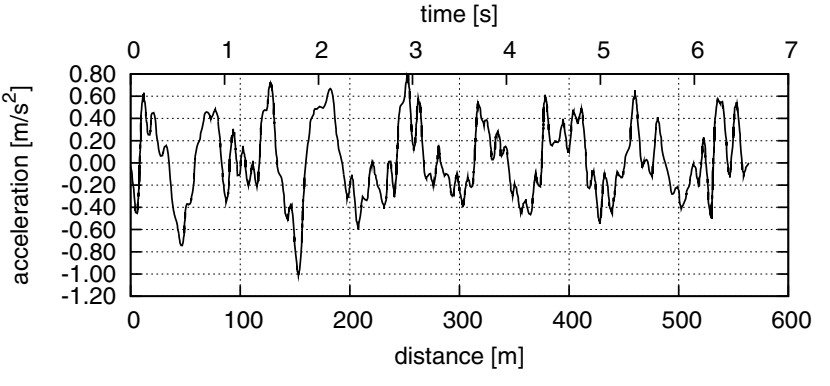


**Fig. 10.7** Accelerations of the body of an ETR500 car at a speed of 290 km/h taken from [42]—deformable bodies model.

## 10.2 Dynamics of the System Vehicle—Y-Type Track

Ballastless tracks and steel sleeper wedge tracks (also called Y-type sleepers) are an example of a dynamic track–vehicle system. Modernization, for reasons of the security of the suspension system and due to the high demands of railway rules, is rarely applied and requires a long and costly research of its prototypes. The modernization of old railway tracks using new technologies gives a noticeable improvement in the dynamic collaboration of the wheel–rail system. The line Plaszow Cracov–Auschwitz is an example where part of the track was made with steel Y-type sleepers. This type of sleeper is also used by the funicular railway to Gubałówka in Zakopane (Figure 10.8) and in Krynica Górska. This scheme compared with a classical track is depicted in Figure 10.9.

**Fig. 10.8** Y-type track.

The advantage of Y-type sleepers is an increase in the lateral stiffness and inertia of the track by including ballast which collaborates with the steel sections (Figure 10.10). This is especially important on curves and in mountain areas. The disadvantage is its higher implementation cost. Measurements on experimental sections show a significant reduction in noise at train crossings.

While the construction of trial road maintenance sections is time-consuming, computer simulations can be done quickly. They are valuable when the analysed model corresponds to the physical model as closely as possible [132, 51]. In its development, the issue is to determine what portion of the wheel weight in contact

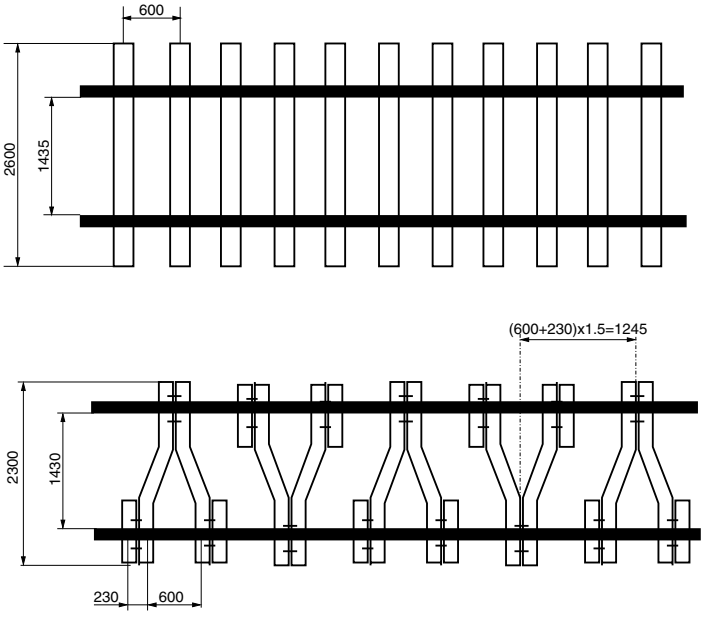


**Fig. 10.9** The track with classical and Y-type sleepers.

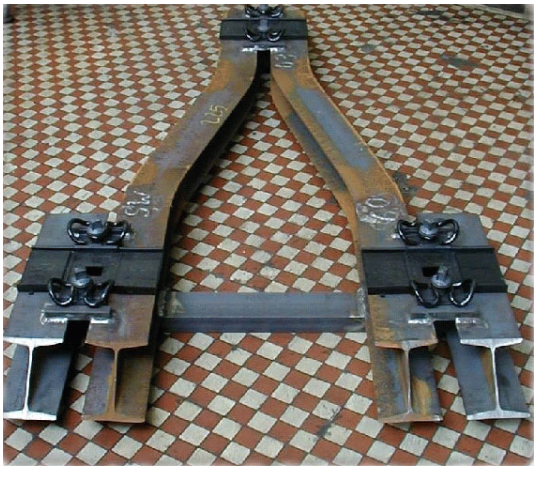

**Fig. 10.10** Wedge steel sleeper.

with the rail dynamically interacts with it. Other parameters of the model can be relatively well-chosen on the basis of the technical documentation. It is certain that at high speeds, the track should not be loaded by only nonlinertial spring elements, and the mass should be taken into account, on which we can then place even a complex vehicle model.

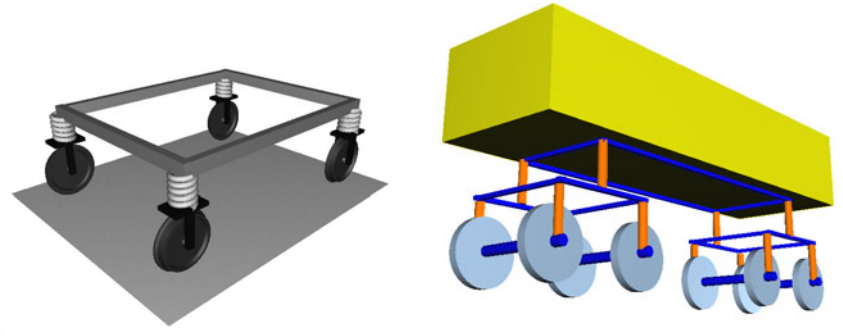

**Fig. 10.11** Model of the track and rail vehicle scheme adopted in numerical computations.

The task of passing a rail vehicle over the track of a classic or Y-type is considered as a problem of two subsystems. The first one is a track consisting of rails, sleepers, viscoelastic pads, and viscoelastic soil. The second subsystem is a rail vehicle, built in a simple way of oscillators, connected by a deformable frame (Figure 10.11). We assume that vibrations of both rails are coupled by the wheelsets, and that the element which couples the vibrations that propagate along the rail is the rail vehicle boogie frame. Rails, sleepers, and the boogie frame, are taken as the grid elements, with three degrees of freedom at a node. Elastic spacers were adopted for the finite elements of a rod. The soil was taken as an inertial Winkler foundation. The frame rigidity and inertia of the individual elements were suitably chosen. In the case of a simplified model of the vehicle in which the wheels are granulated masses, the mass of the wheel, which is accompanied by transverse displacements of the rails, were chosen within the range of 15%–50% by weight of the wheel. Both dynamical systems were solved independently, by building and solving the corresponding systems of algebraic equations. The grid nodes of both discrete systems moved relative to each other and therefore a simple iterative procedure of balancing the forces in both systems was natural to begin with. In the first stage, the track was subjected at the contact points of the wheels with the rails, to forces corresponding to the pressure of the dynamic forces of the boogie wheels. The result was a vertical displacement of a discretized rail element. This allowed of determining the vertical displacements of

the rail at the points of contact with the wheels. These displacements were taken into account as the boundary conditions in the solution of the boogie subjected to external forces, such as its own weight and the weight of the wagon body. The reactions at the points of contact with the rails were the result of solving this stage. These reactions, with opposite signs, were used again to load the track. Iteratively repeating the procedure conducted us in several steps to balance the static system and then let go to the next while in a dynamic process. The procedure worked correctly within a certain range of parameters. In our case, in practice, no loss of stability of the solution occured unless the time step was too large.

Figure 10.12 compares the vertical displacements during the passage of a wheelset at different speeds. The results obtained by the space–time element method were compared with the results of the Medyna package. Despite the strongly differing approaches for creating numerical models, similar results were obtained. One of the exceptions observed, at a speed of 72 km/h and higher, was a beat. We can expect the occurrence of this phenomenon in the results of Medyna at a different speed. This difference may result from a rejection in Medyna of the weight of the wheels associated with the transverse motion of the rails. The three-dimensional image of distorted rail axes at successive moments are shown in Figure 10.13. We see higher amplitudes of displacements of the classical track, especially visible at a distance from the rail vehicle wheels. In order to make a comparison, the results of the measurements recorded in Germany are depicted in Figure 10.14. In addition to the displacements in time showing the average values, similar to the quasistatic case, the values diminished by static deflection are also presented.

Two characteristic cases of the analysis of Y-type sleepers were selected. The rolling of a vehicle with regular, perfect wheels was the first. A vehicle with polygonised, corrugated wheels, which subjected the track to oscillating forces, was the second. The initial stage of rolling on the rails was an excitation of the system. The response of the wheelset/track system depends on the velocity. In the higher velocity range, in the case of perfect wheels, the sleeper type has a significant influence (Figure 10.15).

The second case of the problem is depicted in Figure 10.16. We notice a higher level of oscillations for the Y-type sleepers. However, the average level of displacements is considerably lower. Moreover, with increasing train velocity the amplitudes in both cases start to become similar.

In addition to the improved dynamic properties registered at the rail level, one can see that there are smaller amplitudes of the selected point on the frame of a rail vehicle. The differences between passage on the classical track and the Y-type track is significant and amounts to tens of percent (Figure 10.17).

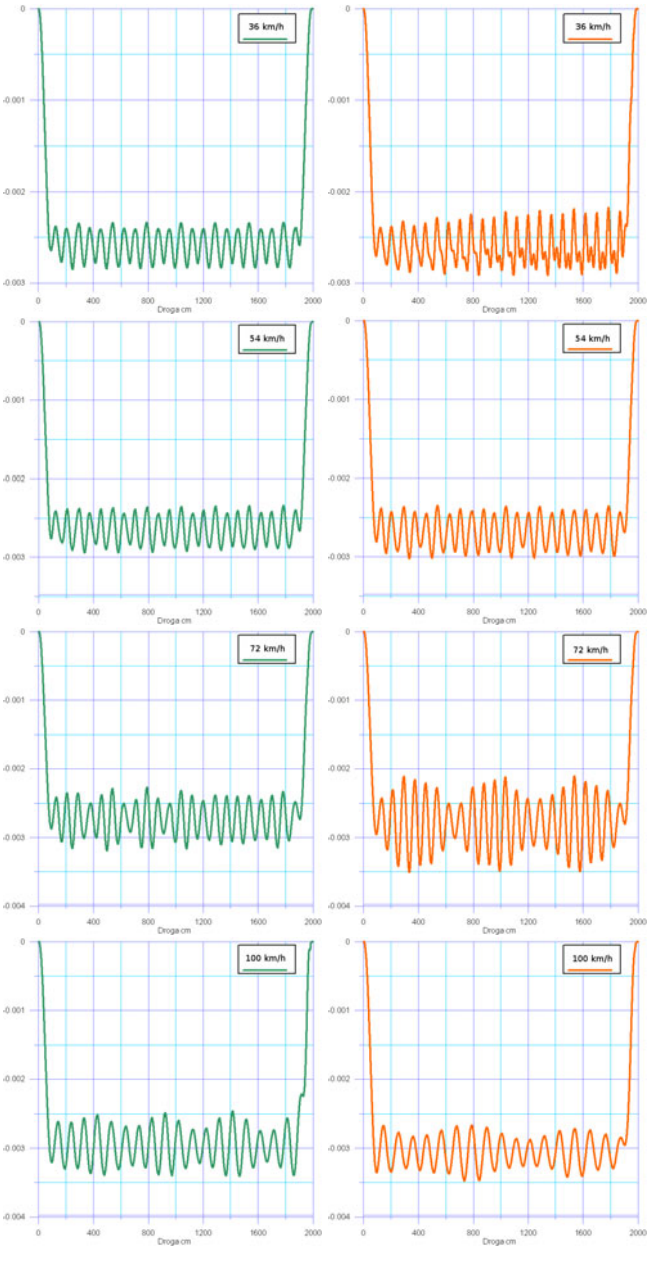


**Fig. 10.12** Vertical displacements of the contact point of the wheel and the rail computed with the package Medyna (left column) and by the space–time element method (right column) at 36, 54, 72 and 100 km/h.

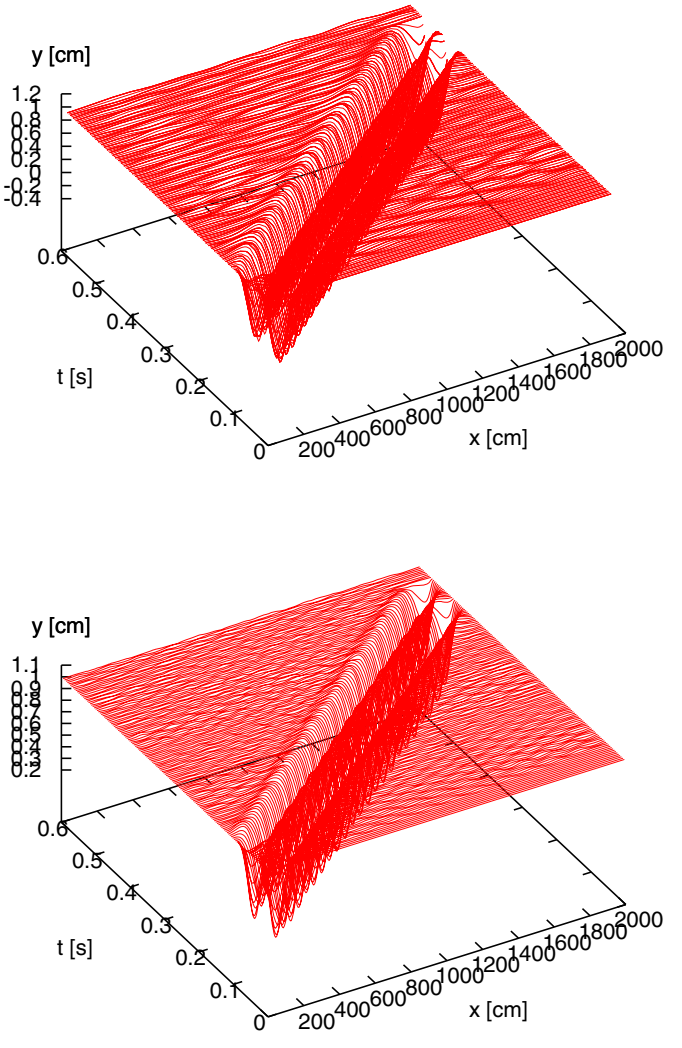


**Fig. 10.13** Vertical displacements of a classical (left) and Y-type track (right) in time-space, loaded by a boogie moving at a speed of 40 m/s.

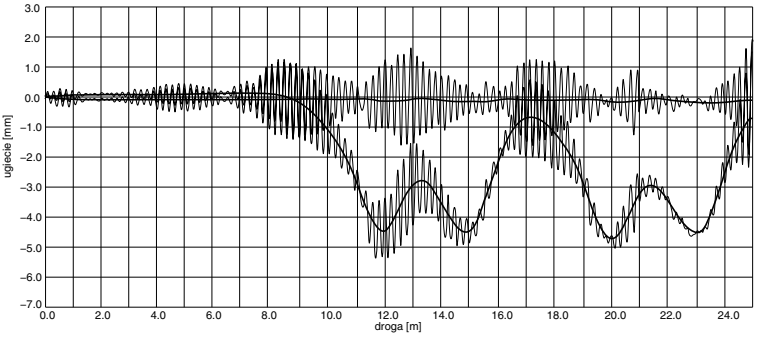


**Fig. 10.14** Measurements of vertical displacements of rails in passage at a speed of 60 km/h and diminished by static deflection.

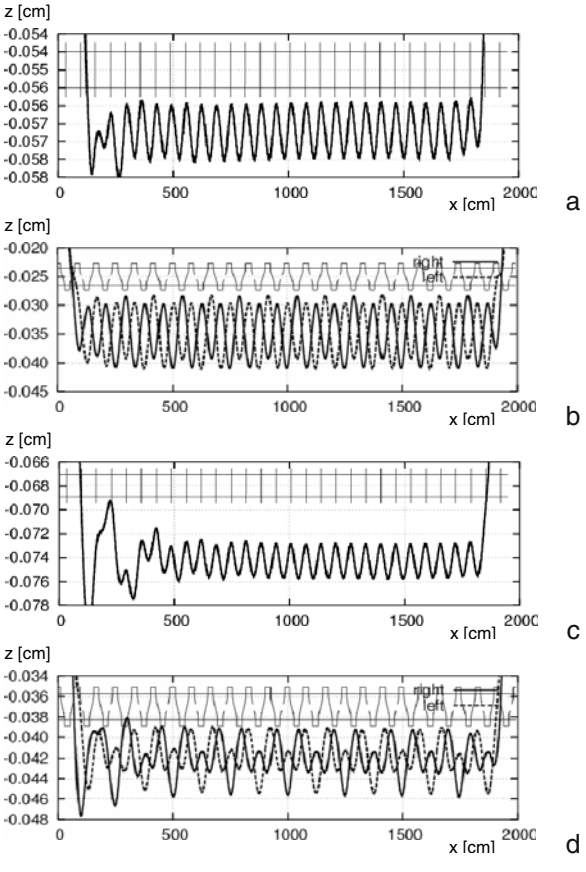


**Fig. 10.15** The vertical displacement of contact points while driving at a speed of 30 m/s (a and b) and 50 m/s (c and d).

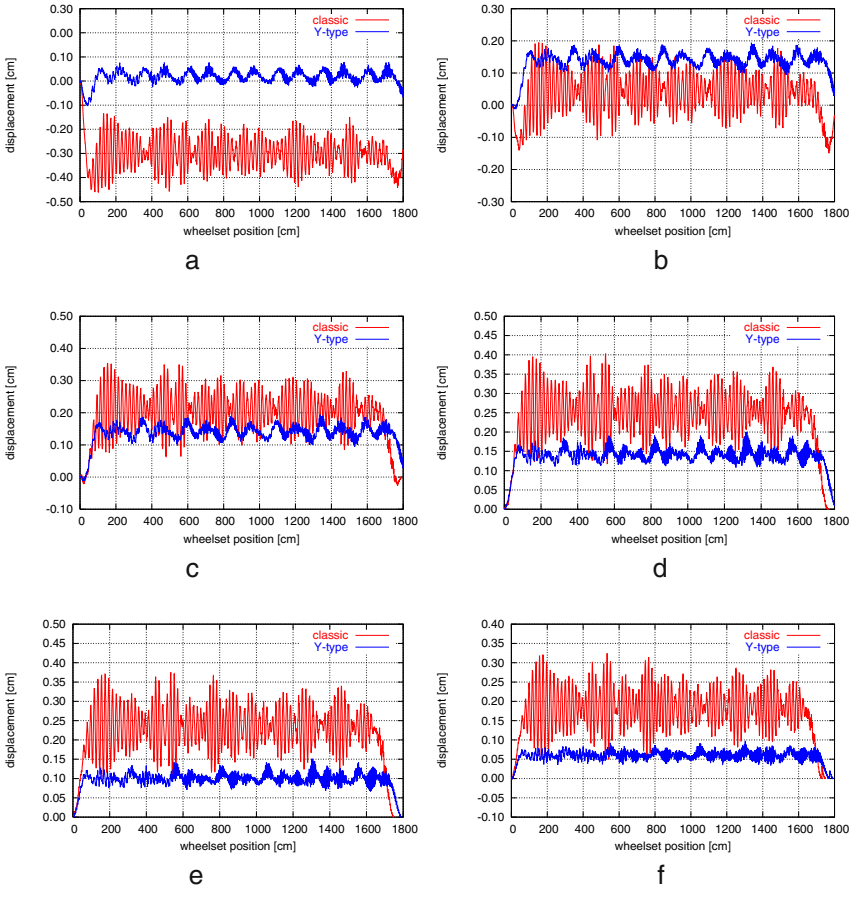


**Fig. 10.16** Vertical displacements recorded at distance of (a) 120 cm, (b) 140 cm, (c) 160 cm, (d) 180 cm, (e) 200 cm, and (f) 220 cm from the contact point of the first wheelset of the boogie with a classical track and with Y-type sleepers at a speed of 40 m/s.

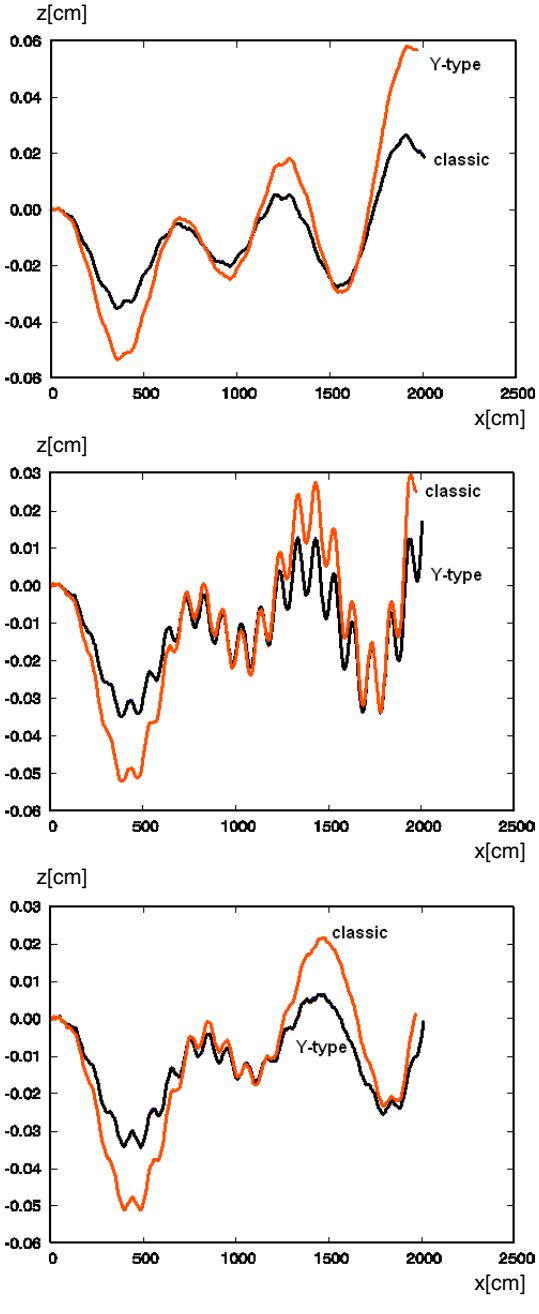


**Fig. 10.17** The vertical displacement of the vehicle frame at a speed of 30, 34, and 36 m/s.

## 10.3 Dynamics of Subway Track

Analysis of the passage of subways aims at assessing the harmful effects of vibrations on the environment. This applies to both passengers and residents of nearby buildings. Harm can be on the one hand loud and annoying sounds at low frequencies, and on the other hand, vibrations causing uneven settling of the foundations of buildings and plaster scratch. For the human ear, the sound of two modal components, with frequencies close to each other, is more annoying than a single frequency, even one with a higher amplitude. The increase in travel speed of subway carriages increases the amplitudes of the vibrations transmitted to the surroundings. Existing subway tunnels can not be rebuilt. We also can not institute any profound vibroacoustic isolation. However, we can try to influence the dynamics of the vehicle–track system by modifying the dynamic characteristics of the rail vehicle or by changing the foundation of the track in the underground tunnel. One such attempt to modify the tracks is presented below.

The idea of the computations was to estimate the influence of different types of vibration isolation on the level of vibrations transmitted to environment. The efficiency of vibration damping together with an analysis of the economic cost of the foundation could indicate the proper treatment of the problem to engineers. Two methods of isolation of the rails from the outer part of the subway tunnel are depicted in Figures 10.18 and 10.19. In the first one, a large area of the cross section of the concrete base is isolated by a viscoelastic mat. We call this, deep isolation. This solution can only be implemented during construction of the tunnel. Later than that, only a second solution can be applied: part of the concrete base can be replaced with a longitudinally placed reinforced beam, isolated by a viscoelastic mat.

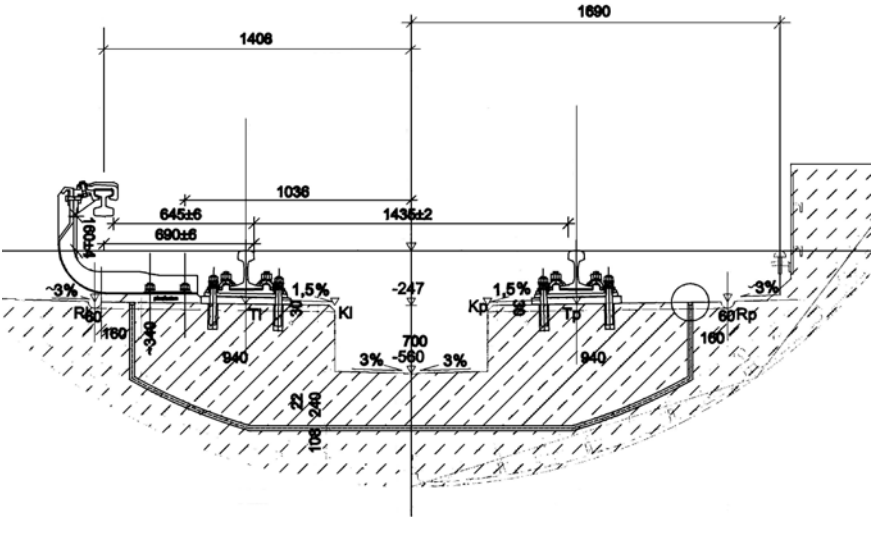


**Fig. 10.18** Subway track with deep isolation.

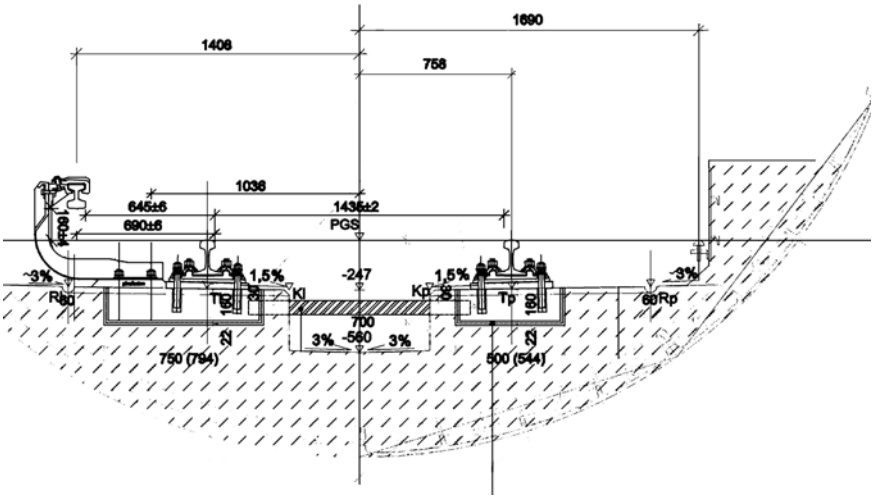


**Fig. 10.19** Subway track with shallow isolation.

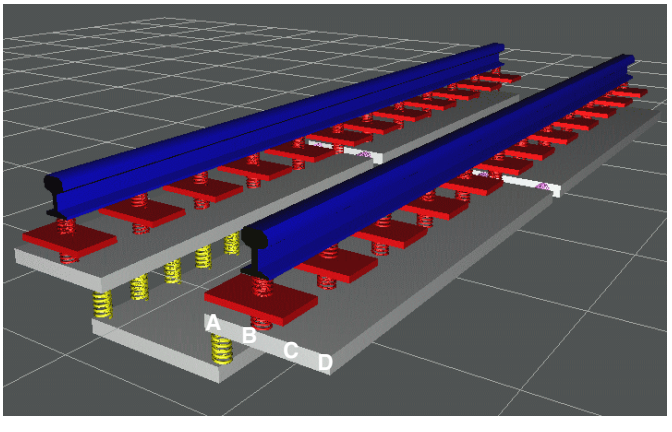


**Fig. 10.20** Model of subway track.

This method is called shallow isolation. The idea is to transfer the dynamic effects from the points of local contact of the wheels with the rails to a larger area of the track. The arrangement of the longitudinal beams under the sleepers so as to be isolated from the foundation further increases the inertia of the vehicle–rail–sleepers interfaces and is a kind of dynamic absorber. The selection of the cross-section of the longitudinal beam and the shallow insulation should take into account, in addition to the dynamic properties of the system components (especially the suspension, mass distribution, stiffness of elastic pads, or rail fastening), also the speed of travel on particular intervals of track.

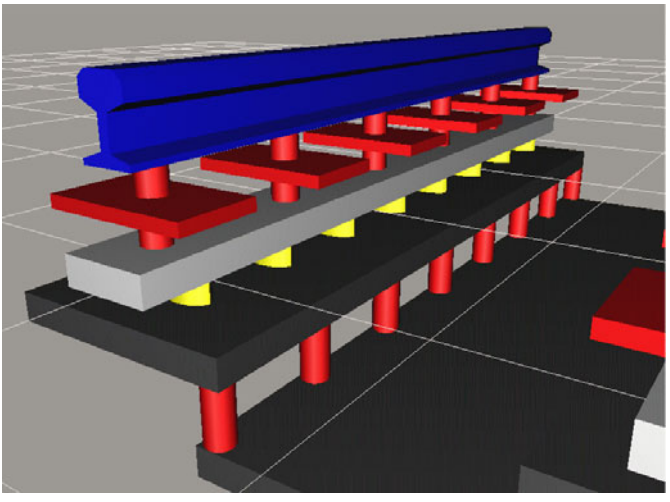

**Fig. 10.21** Shallow isolation of the subway track.

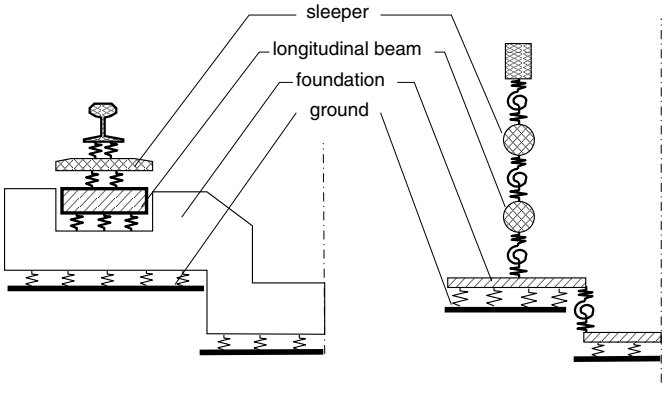


**Fig. 10.22** Modification of the subway track.

The basic simplified numerical model is built as shown in Figure 10.20. Then the model is modified according to the type of isolation. The scheme has been extended to a bar situated under the sleepers, insulated from the substrate with an elastic layer. Such a scheme has allowed of analysing the possibility of isolating the basic layout of the track from the environment. The vibrations caused by passing vehicles, and especially the coupling of the vibrations caused by successive axles, can thus be significantly reduced. In the particular case of adopting a little stiffness of the longitudinal beam, one can reduce the extended problem to the basic scheme. The numerical model was described by the following types of elements: the grid—applied to the rails and sleepers, beams—as applied to the longitudinal beams, plates—describing the foundation and the elastic-viscous Winkler substrate

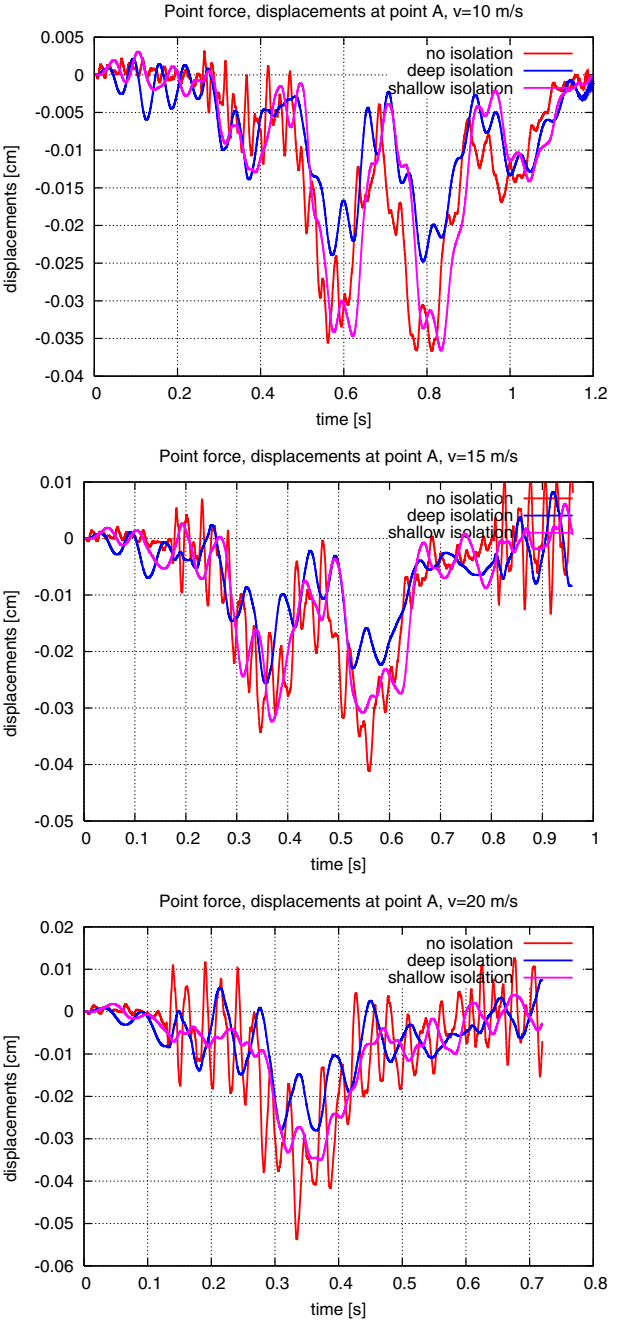


**Fig. 10.23** The reaction under the foundation slab with various types of vibration isolation, at speeds of 10, 15, and 20 m/s.

which describes the type of soil. The spacers were modelled by visco-elastic elements. The plates of the foundation of the track were combined with the spring elements with the possibility of elastic rotation. A relatively simple model of the track describes the real task well. The moving (driving) mass associated with the beam (rail) was taken into account. This is important for correctly formulating the model and the numerical values of the results. The computational model of shallow isolation is depicted in Figures 10.21 and 10.22.

Examples of the reaction at the nodal point under the foundation slab are shown in Figure 10.23. The values of the forces in the case of deep vibration isolation, shallow isolation, and without isolation, are compared. At low speeds, the shallow mat does not make a visible change. At higher speeds, its role begins to emerge. A deep mat improves performance throughout the range of speeds.

## 10.4 Vibrations of Airport Runways

Runways plates are unusual structures. Their thickness reaches 2 m. Moreover, this is a layered structure, consisting of two plates separated by a thin layer of insulation. The load is a set of point-applied forces, moving at high speed. The problem is the distortion caused by temperature changes (Figure 10.24) which cause stresses and by the dynamically applied external load. The temperature gradient reaches 0.08 °C per mm of plate thickness. The heating and cooling of the surface on sunny days causes changes in the altitude of up to several centimeters (Figure 10.25). A plate loaded by deformations induced by heating of the top layer, located on a unilateral elastic foundation, deforms upward. Under the influence of its own weight, long plates fall and break at a certain distance from their ends because of the stress accumulation due to thermal deformations and the load induced by the aircraft (Figure 10.26). This process is repeated, breaking off subsequent segments at the ends. In this way, a continuous plate breaks at regular intervals. The figure shows that a continuous plate will break at each 6 m. To streamline the process, plates are incised at fixed distances to stimulate cracking in the weakened sections. Finally, short plates resist temperature and load stresses and so are considered in the simulations. The problem of dynamic calculations is important because of the large aircraft takeoff weight (for example the mass can reach 600 tons).

It's easy to imagine the physical object, but it is difficult, at the stage of numerical description, to decide how to begin constructing the numerical model. One should consider, e.g., the mutual contact of both concrete slabs. This can be dealt with locally, in the neighbourhood of the point of application of the force. A thick layer of the surface of the concrete slab can be considered as a three-dimensional block. Then, too, there is the ground base, which is usually treated as a set of unilateral constraints. The dilation layer placed between the concrete layers may be grafted adhesively with plates. The plate system is loaded by a system of moving concentrated forces. We should also take into account the air pressure, which is especially important when trying to bond off sealed plate edges from each other and from the ground. We will not go into details of the study of the problem, but will only include

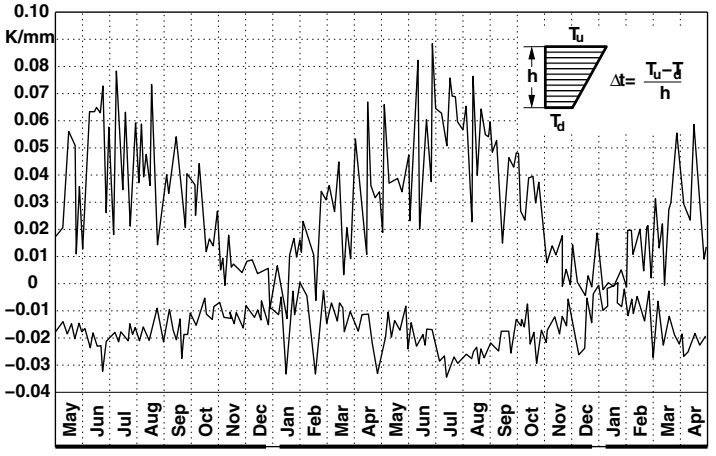


**Fig. 10.24** Annual changes in temperature gradients in the airfield plate during the day (upper graph) and during the night (lower graph).

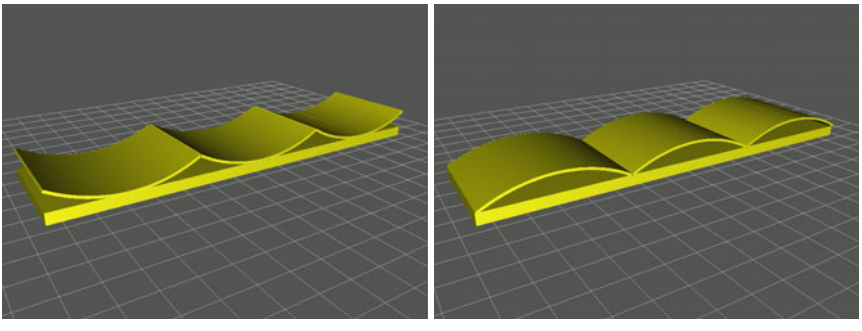

**Fig. 10.25** Deformation of plate segments due to diurnal changes in temperature.

the range of accepted data. The task was described as a pair of plates of medium thickness, bonded with viscoelastic dampers, resting on a Winkler viscoelastic foundation. Vibrations of plates of dimensions 8×8 m were studied. A symmetric half of the task was considered. The loading was performed by an oscillator subjected to a force of 1 MN, moving at speeds of 180–360 km/h (Figure 10.27). The top plate had a thickness of 40 cm, and the lower, 130 cm. Figure 10.28 presents the casting process of the upper plate. The viscoelastic foundation has a stiffness of $k_z = 4 \cdot 10^7$ N/m$^2$, and the dilation mat $E = (0.2–2.0) \cdot 10^{11}$ N/m$^2$. The replacement thickness of the mat equal to 8 cm was assumed in order to take into account the deformation of the concrete block panels in the vertical direction. Figure 10.29 shows the initial state of the simulation. The wave propagation from the source is visible. Let us recall that the symmetric half being considered has dimensions 4×8 m and is relatively narrow. Our figures have disproportionate dimensions. Figure 10.30 shows

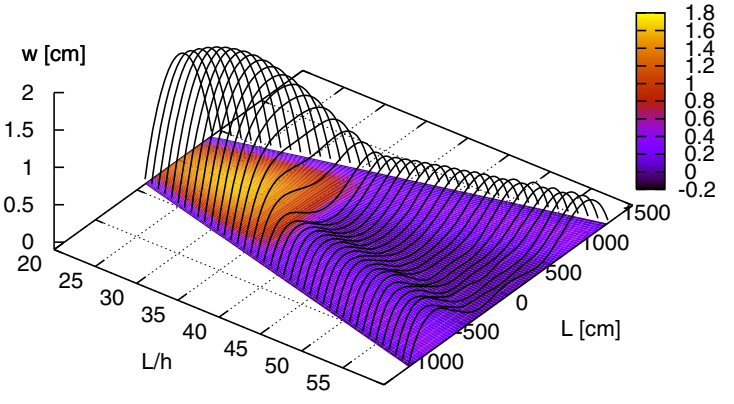


**Fig. 10.26** The deflection line $w$ of the plate deformed by a temperature gradient depending on the length $l$ and ratio of length to thickness $l/h$.

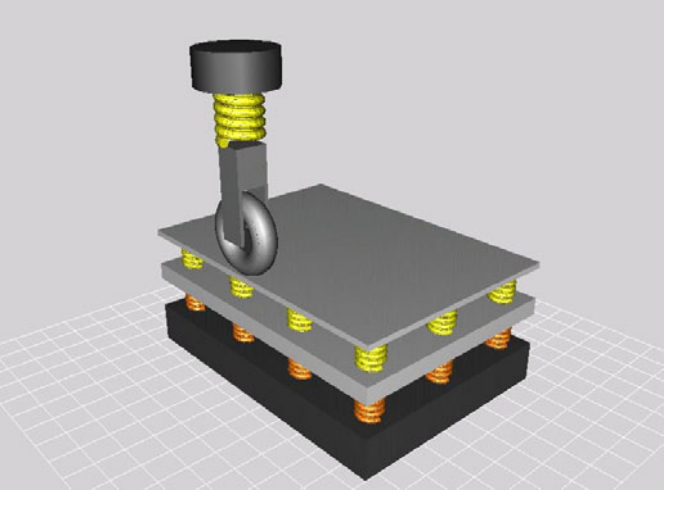

**Fig. 10.27** Diagram of the airfield plate.

**Fig. 10.28** Upper plate construction.

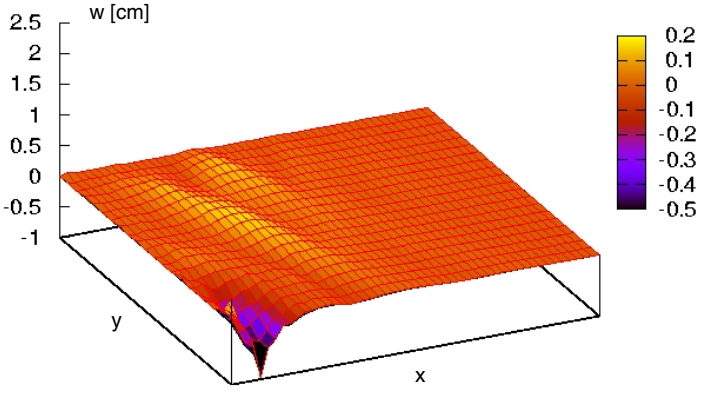


**Fig. 10.29** Wave in the plate in the initial state of the motion.

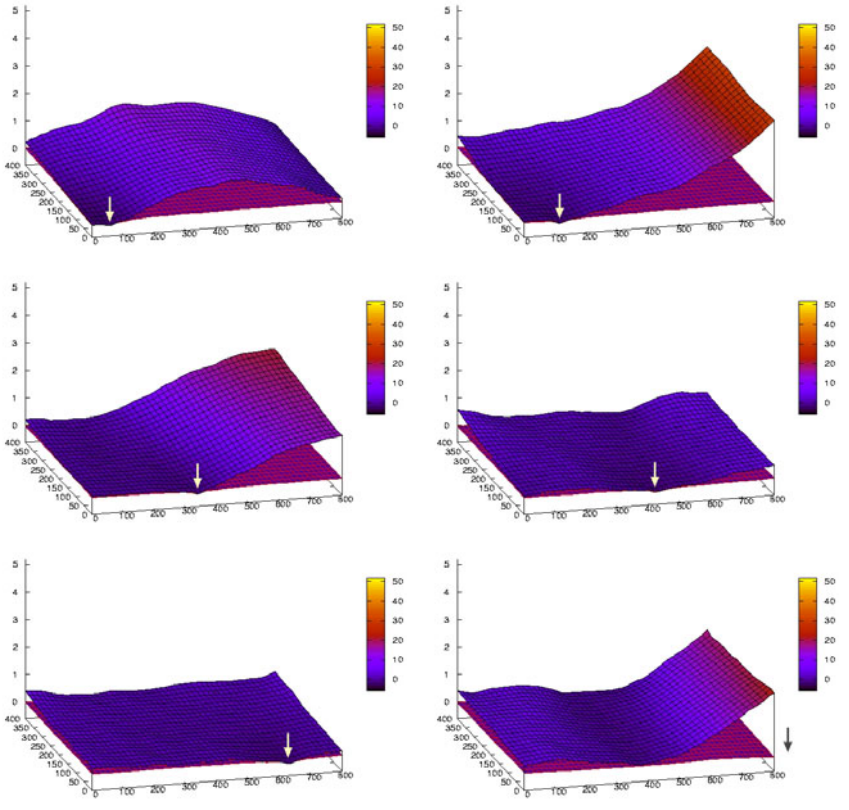

**Fig. 10.30** Successive stages of the passing load.

six phases of the displacement of the system. The loosening of the upper plate is apparent. Two factors determine the image of the displacements: the strength of the dilation layer, i.e., the stress value at which the bonds between the two plates are broken, and the way in which the contact in the zone of force application and stress concentration is modelled. The factors that play a role in a zone limited to a very small loaded area, virtually decide the outcome. That is why the task can not be analysed by limiting attention to a pair of plates. Proper selection of the parameters describing the two decisive factors must be preceded by a three-dimensional static analysis of the strain state.